

Understanding electrokinetics at the nanoscale: A perspective

Hsueh-Chia Chang^{a)} and Gilad Yossifon

Department of Chemical and Biomolecular Engineering, Center for Microfluidics and Medical Diagnostics, University of Notre Dame, Notre Dame, Indiana 46556, USA

(Received 30 November 2008; accepted 2 December 2008; published online 2 January 2009)

Electrokinetics promises to be the microfluidic technique of choice for portable diagnostic chips and for nanofluidic molecular detectors. However, despite two centuries of research, our understanding of ion transport and electro-osmotic flow in and near nanoporous membranes, whose pores are natural nanochannels, remains woefully inadequate. This short exposition reviews the various ion-flux and hydrodynamic anomalies and speculates on their potential applications, particularly in the area of molecular sensing. In the process, we revisit several old disciplines, with some unsolved open questions, and we hope to create a new one. © 2009 American Institute of Physics. [DOI: [10.1063/1.3056045](https://doi.org/10.1063/1.3056045)]

I. INTRODUCTION

There is considerable interest in synthesizing nanoporous membranes on microfluidic chips and fabricating nanochannels directly into chips. Within our group, we have used nanoporous membranes as microfilters for removing debris or concentrating analytes,¹ as substrates for electrokinetic pumps and electrospray emitters into mass spectrometers,² and as effective chromatograph packing.³ The membranes typically have a high surface charge density of about one charge per 10 nm^2 , and when their pore dimension is smaller than the electric Debye layer (EDL) thickness (i.e., there exists a strong EDL overlap), these membranes become ion-selective such that mostly counterions can enter and exit the membrane. As the usual Debye screening is much weaker within their nanopores for the same reason, the permselective membranes allow a high surface adsorption rate of chemical and biological analytes.⁴ These desirable features of nanoporous membranes are extensively exploited in desalination, chromatography,³ virus traps,⁴ etc. and have found similar applications in chip-scale analogs of the same processes.

Electrochemical sensing of molecular hybridization is a rather peculiar form of ion-selective current transport, with the electron-transfer oxidation and reduction reaction occurring at the electrode providing the ion selectivity.⁵ Although a nanochannel or a nanopore is absent in this system, the ion flux across the electrode Debye layer is very similar to that across the interface between the nanochannel and the microreservoir, since both systems exhibit ion permselectivity. The flux in that region will be shown to be current-controlling for both systems.

There are, however, unique microfluidic applications of nanoporous membranes that are not scaled-down versions of large-scale processes. The nanopores contain more space charge per unit volume than microchannels. As such, nanopores generate a high Maxwell pressure per unit volume when an electric field is applied, thus allowing the realization of high pressure ($>5\text{ atm}$) microcapillary electrokinetic pump.² Using streaming potential to generate electricity is also best done with a nanoporous membrane⁶ for precisely the same reason.

The same filtering, concentrating, and flow generating ability of nanoporous membranes can now be mimicked by fabricated nanochannels, which can be easier to introduce onto chips and whose geometry and surface functionalization are easier to modify than nanoporous membranes.⁷

^{a)}Author to whom correspondence should be addressed. Electronic address: hchang@nd.edu.

There are also suggestions of using a nanochannel as an electrochemical molecular sensor, much like what is done with electrode sensors, but with larger selectivity and sensitivity.⁸ Transparent chips allow us to monitor the ion and liquid flux within the channel with uncharged and charged dye.⁹ As such, fabricated nanochannels allow us to explore the ion flux mechanism within nanoporous materials, with some important caveats that will be addressed in this article.

Despite these obvious advantages of nanoporous membranes and nanochannels in electrokinetic chips, ionic and solvent fluxes (current and hydrodynamics) in such media remain poorly understood. We review some anomalous features here and propose fruitful research directions that will allow nano-electrokinetics to blossom into a robust technology for diagnostic and biosensor science.

II. NONLINEAR *I-V* CHARACTERISTICS

The ion flux mechanism across a nanoporous membrane has been known to produce anomalous ion-current dynamics for more than a century.¹⁰ Such anomalous behavior is not just due to Faradaic or ion-exchange reaction within the membrane, and actually spurred forays into irreversible thermodynamics 30 years ago. Even standard ion-selective transport across the nanoporous membrane can exhibit extremely complex steady and dynamic phenomena. Nanoporous membranes are known to store charge¹ because of the conductivity jump at the membrane surface, to produce streaming potentials,⁶ electroviscous effects,⁶ nonlinear *I-V* characteristics, and oscillatory instabilities.¹⁰ Unlike polarized capacitors, such charge buildup can be sustained with a dc field and allows a through current. Hence it endows the nanoporous membrane with dc *I-V* and ac impedance characteristics that cannot be understood through standard electric elements such as resistors, capacitors, and inductors. Not surprisingly, ion channels of cell membranes also exhibit such curious characteristics that are often described as nonlinear resistor elements.¹¹ Many of these anomalies are now transferred to nanochannels but with important modifications. The underlying physics of these anomalies, unfortunately, remain poorly understood despite two centuries of intensive research.

Examples of such anomalies abound. Figure 1 depicts the *I-V* characteristic across a Pyrex glass-polysilicon nanoslit described schematically in the inset. The nanoslit behaves as a linear Ohmic resistor at high ionic strength, when the channel gap is larger than the Debye length. However, it is clearly non-Ohmic at low concentrations, wherein EDLs of both substrates overlap, as it exhibits three distinct regions of constant differential resistance, showing voltage-gating-like nonlinear circuit behavior. An Ohmic region at low voltages is followed (~ 10 V) by a nearly constant-current limiting region and then (~ 23 V) an overlimiting region with a conductance higher than even the Ohmic region. As another example, we show in Fig. 2 the cyclic voltammetry of a similar nanoslit to that described in Fig. 1. Considerable hysteretic behavior is observed and the hysteresis is a strong function of the scan rate. The hysteretic phenomenon occurs despite the fact that there is no discernable reaction within the membrane. Figure 3 shows the ac impedance measurements across the nanoslit at different dc biases, with very chaotic noise at low frequencies at high biases. Even without Faradaic or ion-exchange reaction, the dc and ac ion transport characteristics across the nanoslit are very different from a simple resistor or a resistor-capacitor system.

These nonlinear *I-V* and capacitance charging characteristics are also found across cell membranes, driven by the potential drop across the membrane due to a difference in the ionic strength. The nonlinear *I-V* characteristics of cells, however, are due mostly to voltage-gating effects of ion-channel protein at subnanoscales. Nevertheless, the conductivity gradient across cells can also accumulate charge at its interface to produce cell polarization and dipoles, an empirical fact that has been exploited to sort cells by DEP on chips. The nonlinear *I-V* and capacitance charging features of the cell are used for neuron signal transmission, activating and controlling growth factor-receptor binding, and regulating the pathways of many messenger molecules across the membrane.¹¹ It is our belief that the same nonlinear characteristics in nanochannels and nanoporous membranes will introduce new impedance molecular detection strategies, particularly those for the detection of charged molecules like peptides, RNA, and DNA.

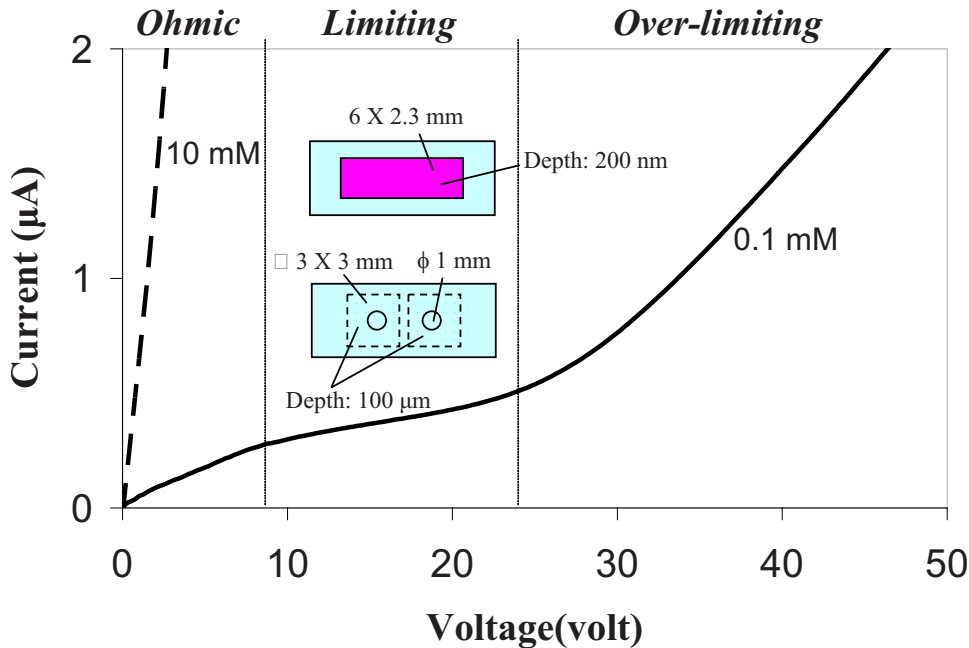


FIG. 1. Nonlinear dc I - V curve across a nanoslit at different electrolyte strengths. The chip is formed by anodic bonding of the two Pyrex glass slides depicted in the inset. The resulting nanoslit dimensions are width $w=2.3$ mm, height $h=200$ nm, and length $d=0.5$ mm, while the two microreservoirs at the end of the nanoslit are squares of about 3×3 mm in length and 0.1 mm in depth.

III. INTRACHANNEL OHMIC RESISTANCE

Some of the relevant ion transport physics behind the curious I - V characteristics are understood. The conductance in the Ohmic region of Fig. 1 is due almost entirely to intrananochannel resistance. This is a clear departure from a nanoporous membrane, whose conductivity is typically

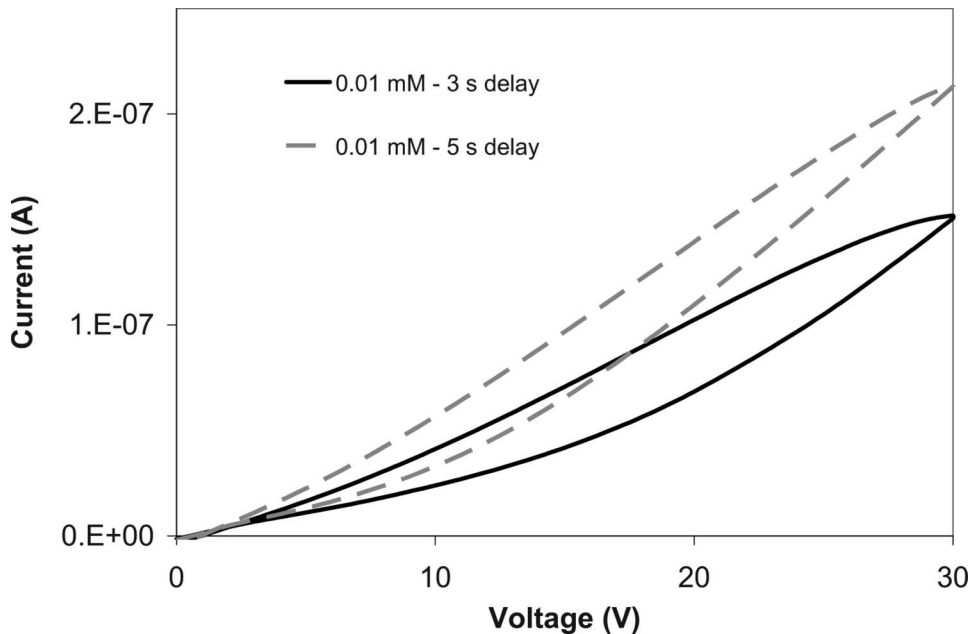


FIG. 2. Cyclic voltammetry across a similar nanoslit to that of Fig. 1 at different scan rates.

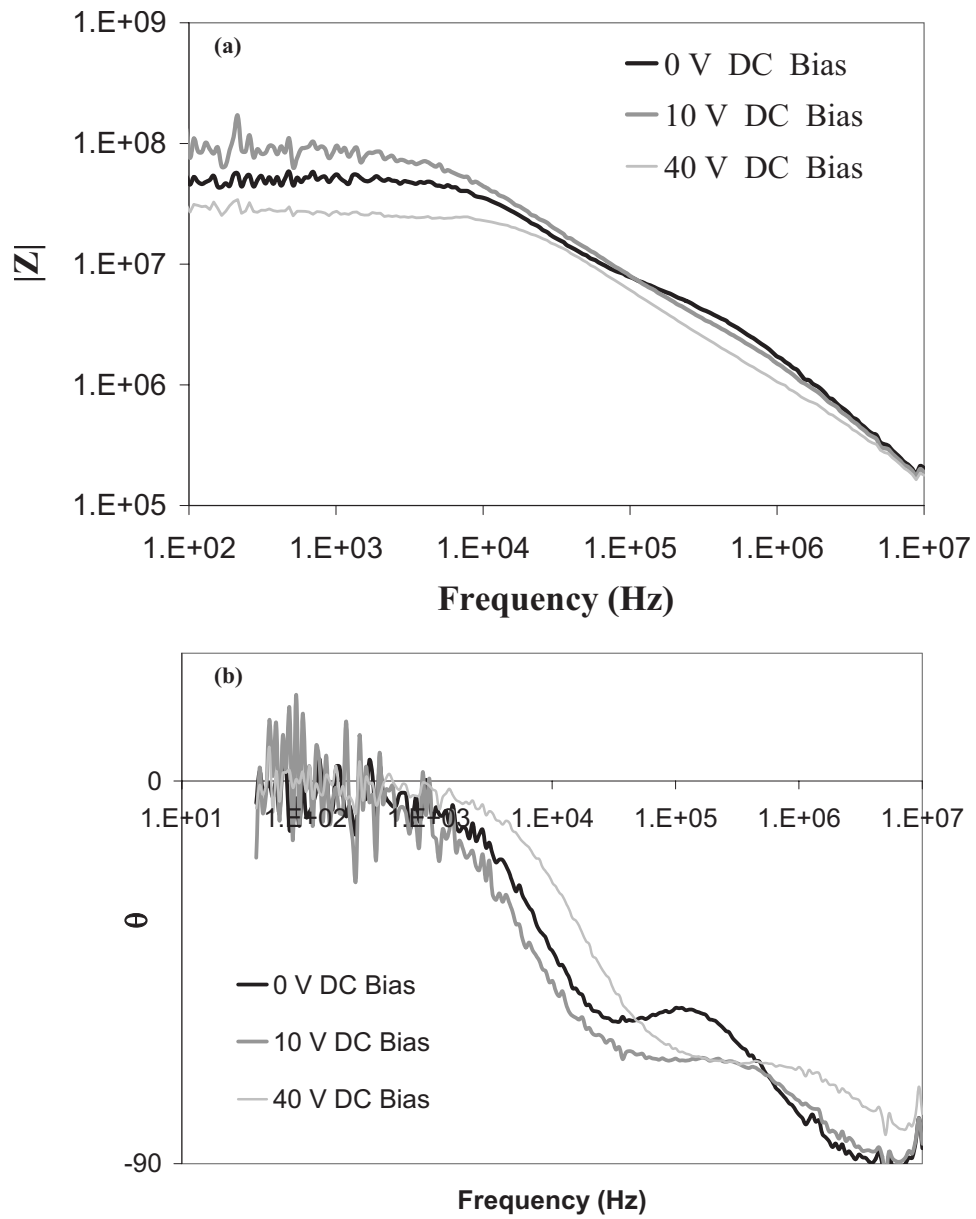


FIG. 3. (a) Magnitude and (b) phase of the ac impedance of the nanoslit in Fig. 1 with different dc biases at an electrolyte strength of 0.1 mM.

assumed to be high and hence offers no resistance to ion current. However, in a nanochannel design like Fig. 1, the cross-section area of the nanochannel is much smaller than that in the connecting microchannel—its ratio is much smaller than the typical porosity of the nanoporous membrane (or the $2/3$ power of it to produce the void cross-section area ratio). The length of the nanochannel is also comparable to the microchannel, whereas a membrane is typically much thinner than the electrode separation. As a result, even with a higher conductivity within the nanochannel, these geometric effects render the conductance of the nanochannel much smaller than the bulk and hence become the bottleneck to ion current. While the idealized Ohmic conditions in the bulk correspond to an electroneutral electrolyte with no concentration gradient, the intrachannel Ohmic resistance is due to mobile ions of the charged electrolyte within the slit.

Stein *et al.*⁷ first realized that, at low ionic strengths, the dc conductance of the nanochannel

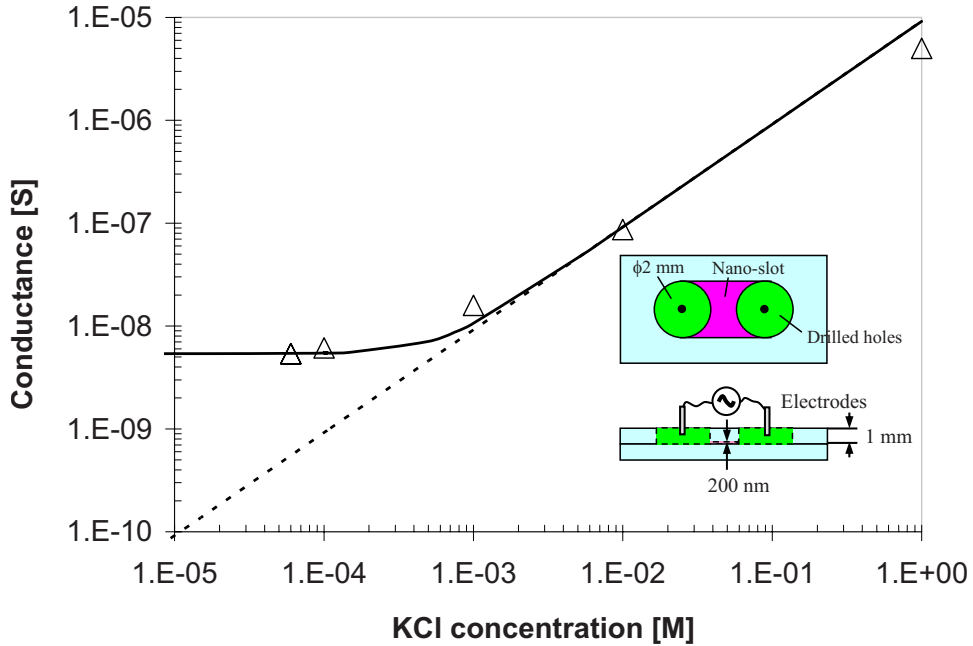


FIG. 4. Nanoslit conductance as a function of the electrolyte concentration (symbols—experiment; continuous line—model (1); dashed line—bulk conductance). The nanoslit (schematically described in the inset) dimensions are width $w=2$ mm, height $h=200$ nm, and length $d\sim 1$ mm.

(essentially the conductance measured across the electrodes at the ends of the microchannel) is independent of the bulk electrolyte concentration. Under such ionic strengths, the double layers on the top and bottom substrates of the nanochannel overlap such that most of the ions in it are counterions. As the nanochannel unit, at relatively low voltages wherein intrachannel polarization is negligible, must be electroneutral, the total number of counterions must be equal to the total constant surface charge and is independent of the bulk ionic strength. As the channel conductivity is proportional to the total ions within the nanochannel and as most of the ions are counterions, the conductance is independent of bulk electrolyte conditions. Simple algebra for the ion concentrations within the nanochannel, which has a Boltzmann dependence on the potential, then produces the Donnan relationship between the nanochannel conductance and the bulk electrolyte concentration¹² (assuming for simplicity a symmetric electrolyte $z^+=-z^-=z$ and equal diffusivities $D^+=D^-=D$),

$$I/V = \left(F^2 \sum z_i^2 \nu_i c_i \right) wh/d = 2F\mu\sqrt{(\Sigma/2)^2 + C_\infty^2} wh/d, \quad (1)$$

where C_∞ is the bulk concentration, w is the width of the channel, h is the height, d is the length, $\mu=zF\nu=zFD/RT$ is the ion mobility, F denotes the Faraday number, R is the universal gas constant, T is the absolute temperature, and $\Sigma [= -2\sigma/(zFh)]$ is the effective fixed volumetric charge. In the limit of low bulk concentration, the Debye layers overlap across the nanochannel such that it contains mostly counterions. The electroneutrality condition then stipulates that the total number of counterions responsible for the conductance is equal to the total surface charge. This C_∞ -independent limit is evident in Eq. (1) and so is the high C_∞ limit when the conductivity approaches that of the bulk and hence increases linearly with C_∞ . The unknown surface charge density, σ , can be fitted by the low-ionic strength asymptote. This is done in Fig. 4 for the low-voltage Ohmic regions of Fig. 1. A reasonable surface charge density of ~ 8 mC/m² for Pyrex glass-polysilicon combination is found to quantitatively capture the channel conductance for all electrolyte conditions.

At high conductivities, there is no ion-selectivity within the nanoslit, as its double layers do not overlap. As such, the electrolyte within the nanochannel is mostly electroneutral and equal in concentration to the bulk electrolyte. Intrachannel resistance also controls the current flux due to field-focusing. As is true for all electroneutral and spatially homogeneous electrolyte systems, the *I-V* characteristics of the nanoslit at high conductivities are hence Ohmic with a linear dependence between current and voltage. The ionic strength within the nanoslit begins to deviate from the bulk conditions at low bulk concentrations (Fig. 4) and the fluid within the nanoslit exhibits a net ionic charge due to ion selectivity. Nevertheless, at sufficiently low voltages, the nanoslit and the bulk conductivities remain homogeneous in the flux direction and they can still be modeled as two resistors in series, with the intraslit resistance dominating in most cases due to field focusing effects.¹²

IV. NON-OHMIC RESISTANCE DUE TO ENTRANCE/SURFACE POLARIZATION

In the classical membrane current theories, the Ohmic region is believed to terminate at sufficiently high voltage when the current density approaches a near-constant limiting current value, seen in the intermediate voltage region of Fig. 1. Due to electrostatic attraction between surface charges and counterions in the membrane, the membrane is locally electroneutral, at least at low voltages when there is no internal polarization. Consequently, an intramembrane spatial gradient in the counterion concentration cannot be established at low voltages. This is not true, however, in the bulk, and diffusion due to concentration gradient can augment electromigration in the electroneutral bulk. This region with a large concentration gradient remains electroneutral due to the strong attraction between the counterions and coions—it is just that neither is immobilized and hence required to be spatially homogeneous. A strong concentration gradient is known to exist at least in some part of the bulk electrolyte.¹³ This diffusion layer where the concentration gradient exists can be the entire bulk region between the membrane and the electrode or it can be over a small region near the membrane because of convection and stirring effects. However, the concentration gradient can reduce the electrolyte concentration near the membrane surface and hence reduce the bulk conductivity. At low voltages, the bulk concentration gradient is not pronounced, as bulk electromigration is sufficient to sustain a counterion flux to the rate-limiting intramembrane conduction, which is responsible for the Ohmic region at low voltages in Fig. 1. The concentration gradient becomes more pronounced at higher voltages and begins to reduce the electrolyte conductivity near the membrane, thus shifting the current controlling region from the membrane to the bulk. In fact, Ben and Chang¹⁶ showed that any electroneutral diffusion layer with a linear concentration profile also sustains a potential drop that is the logarithm of the concentration drop across it, which is due to the fact that the coion is at Boltzmann equilibrium. Hence, a larger voltage does not necessarily drive more current, as the potential drop is used to sustain an equilibrium concentration gradient and not an open ion flux. The differential conductivity begins to decrease from the Ohmic value, as seen in Fig. 1 (at ~ 10 V), when ion transport starts to be controlled by this diffusion layer as the interfacial concentration of the diffusion layer approaches zero. According to Levich's theory,¹³ the limiting current occurs when the ion concentration at the membrane-electrolyte interface approaches zero such that the ion flux cannot be increased beyond that. At this limit, a simple analysis of the diffusion layer shows that the electromigration flux is equal to the diffusive flux and hence Levich's limiting current density is simply $2FzDC_\infty/L$, where L is the thickness of the diffusion layer. Near the limiting-current region, it is the diffusion layer that controls the current and voltage drop and not the nanoslit, which controls in the Ohmic region. There is no known analog of this diffusion layer in electric circuits, as the diffusivity of electrons or holes is typically too high to allow an electroneutral concentration gradient to be established. This diffusion-layer endowed limiting-current phenomenon would hence be one of the anomalous current flux phenomena of nanoporous membranes, as viewed from the perspective of electric circuit theory.

There are, however, several empirical contradictions and conceptual inconsistencies with this theory. It is the differential resistance that is observed to approach another high constant asymptote beyond the Ohmic region, rather than the current density, as seen in Fig. 1. Levich's theory does

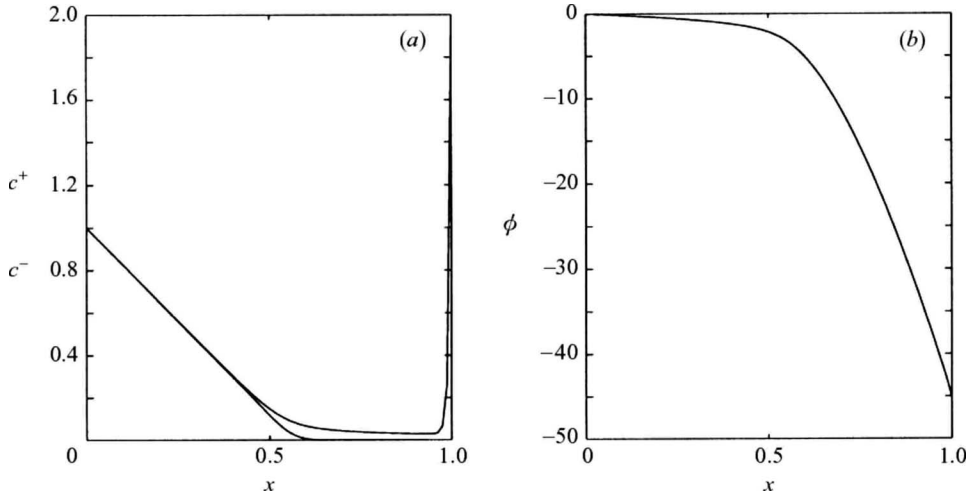


FIG. 5. Extended polarized layer at the surface of a membrane. The spatial coordinate x has been normalized by the thickness of the diffusion layer, which is arbitrarily imposed. An electroneutral diffusion layer region is seen on the left with a linear concentration profile (a) and a logarithm potential drop (b). Within it lies an extended polarized layer with an excess of cations, which are the counterions. A near equilibrium Poisson–Boltzmann region is observed next to the membrane. The external diffusion layer can extend to the electrode or can terminate a short distance from the membrane (Reprinted with permission—Ref. 16).

not offer a theory for the thickness L of this diffusion layer. Some have attributed it to the usual convection-diffusion boundary layer in the presence of vigorous stirring or external flow.¹⁴ However, with stagnant fluids in the microchannel, it is most likely that the diffusion layer spans the entire region between the membrane and the electrode. If so, why does a third overlimiting region exists at high voltage, with a differential conductance much higher than any other region at lower voltages (Fig. 1)? There is clearly yet another mechanism at play that selects the diffusion layer thickness L , which is unique to nanoporous membranes.

Rubinstein and Shtilman¹⁵ were the first to suggest that ion flux into the nanoporous membrane can not be enhanced by the development of a diffusion layer alone necessitates also the emergence of an extended polarized layer, another deviation from the electroneutral Ohmic condition. This polarized layer resides within the concentration-polarization layer, between the thin Debye layer, and the electroneutral diffusion layer with a linear concentration profile, and contains space charge due to a net excess of counterions. This existence of a net charged layer on the depleted side of the membrane amplifies the applied electric field and drives a large electromigrative flux that, together with the large concentration gradient within the electroneutral diffusion layer, prevents the current density from saturating at Levich's limiting current density. The charged layer is not at Boltzmann equilibrium and, unlike that in the diffusion layer, its potential drop drives a net flux. It also diminishes the diffusion layer thickness and hence increases the flux across the rate-limiting diffusion layer. The same polarization and concentration depletion that amplifies the electric field at the entrance of the nanoslit also renders the intrachannel resistance insignificant and the bottleneck to ion flux occurs at the polarized layer. Hence, Levich's limiting current density theory is not strictly correct. The extended polarized layer increases in length with voltage and so does the current density. Instead of a limiting-current density, one has a limiting differential conductance or impedance in this intermediate region.

An extended polarized layer with space charge that nevertheless sustains a through current flux has no analog in electric circuit theory, not even leaky dielectric models that allow surface currents. This is yet another departure for ion flux across nanoporous membranes from conventional circuit elements for electrons or holes. The structure of this extended polarized layer is now well characterized, and we show in Fig. 5 a typical structure in the overlimiting region from Ben and Chang¹⁶ for a given diffusion layer thickness.

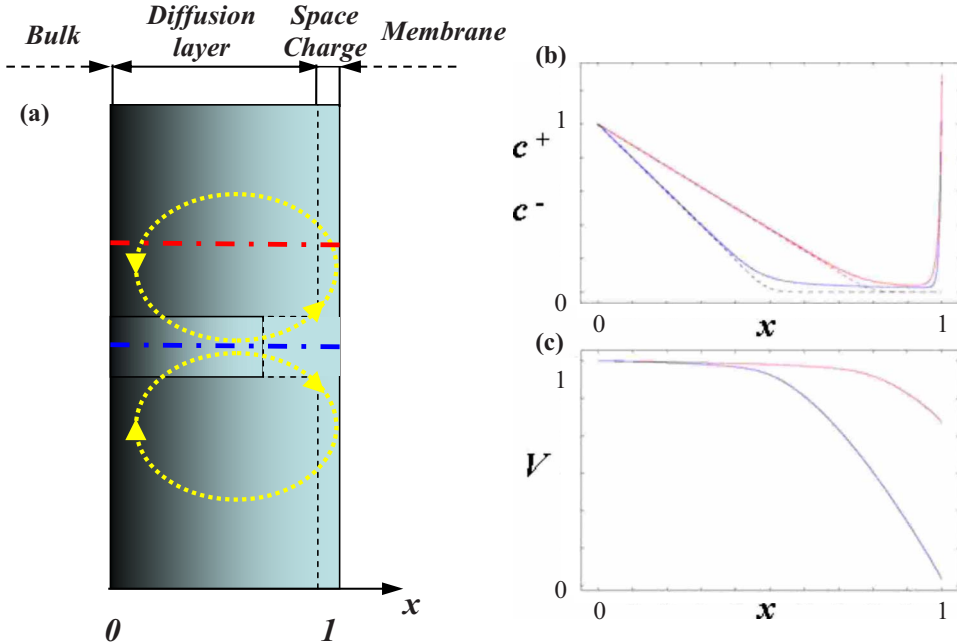


FIG. 6. Schematics of Rubinstein's instability physical mechanism: (a) a small perturbation of the extended polarized layer thickness (increased thickness at the center) resulting in transverse Maxwell pressure gradients that lead to a vortex pair in a positive feedback loop; (b) concentration profiles (normalized by the bulk concentration) of the different ionic species; and (c) electric potential profile (normalized by the applied voltage) across the center (blue line) and off-center (red line) of the perturbation region.

Nevertheless, since the polarized layer is in series with the electroneutral diffusion layer, the current flux across both should be the same. It is then curious that the overlimiting region has an almost discontinuous differential conductance from that in the intermediate limiting-resistance region. Rubinstein *et al.*¹⁷ suggested that the diffusion layer thickness L in the overlimiting region is much smaller than the distance to the electrode, which is the diffusion layer for the Ohmic and limiting-resistance regions, because of a vortex instability. This would explain why the overlimiting differential resistance can be the lowest of all three regions—it has the benefit of a very thin diffusion layer and a correspondingly thin polarized layer, none of which is present in the Ohmic region. The space-charge layer on the outside of the membrane/nanochannel becomes unstable only beyond another critical voltage (larger than that for the emergence of the polarized layer when a transition from the Ohmic to the limiting-resistance regions occurs) when lateral variations in the Maxwell pressure gradient produce a vertical flow that convects electroneutral bulk solution into regions with larger polarization (and hence higher osmotic pressures), thus reducing the diffusion layer further to effect a positive feedback loop (Fig. 6). That a critical voltage, which depends on the microchannel dimensions, exists is because flow resistance in a microchannel necessitates a critical driving force for the vertical flow, as in classical Rayleigh–Benard instabilities within a slot.

V. VOLTAGE-GATING AND VORTEX-INSTABILITY

We have recently verified this scenario by Rubinstein and co-workers¹⁸ using fluorescent dye and confocal imaging to observe the depletion layer. As shown in the images of Fig. 7 with parallel current measurements (similar to Fig. 1), the overlimiting current is only detected beyond a critical voltage (>20 V) when the vortices also appear. The dc I - V characteristics of a nanoporous membrane is hence sensitively affected by hydrodynamics—another feature absent in electric elements.

This hydrodynamic enhanced instability produces the voltage-gating type I - V characteristic of

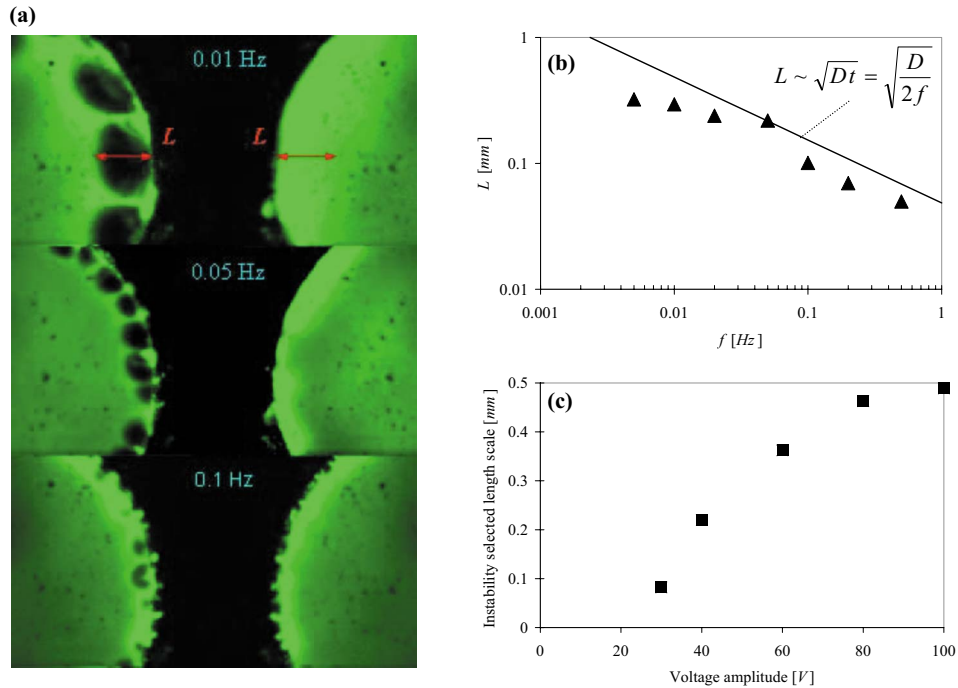


FIG. 7. Rubinstein's vortex instability in front of the nanoslit in Fig. 4 develops beyond a critical voltage to select a thin diffusion layer much shorter than the distance to the electrode. (a) The confocal images are taken at 40 V showing vortices at the depletion layer on the anodic side (left reservoir) for an ionic strength of ~ 0.1 mM. The diffusion layer is allowed to grow to a certain thickness with a low-frequency ac field and the vortices only appear when the frequency is below 0.1 Hz and when the voltage is beyond ~ 20 V (enhanced online). (b) A Log-Log graph of the maximum extent of the experimentally measured L vs the frequency. A clear break from the diffusive scaling, \sqrt{Dt} (continuous line), occurs at a frequency smaller than 0.05 Hz corresponding to the instability selected length scale. (c) The thickness of the instability selected diffusion layer is recorded for each voltage. Below 20 V, the diffusion layer essentially extends to the electrode (Reprinted with permission—Ref. 18).

Fig. 1. Since the polarized layer appears only beyond a critical voltage and the vortex instability onset is controlled by an overvoltage,¹⁹ the high-current density of the latter occurs only beyond a second critical voltage. The vortices act as a gating electrode to enhance the ion flux across the channel.

There is some confusion between Rubinstein's vortex instability and Dukhin's vortices generated by curved or composite interfaces.¹⁴ Both involve the extended polarized layer outside conducting nanoporous membranes. However, Rubinstein's vortices originate from an internal instability and can develop even for a planar interface beyond a critical voltage. Dukhin's vortices, however, rely on the polarization gradient on a curved surface (typically an ion exchange granule) or a heterogeneous membrane and occur for any voltage beyond the first critical voltage for the emergence of the extended polarized layer, in contrast to Rubinstein's instability onset, which necessitates an overvoltage, i.e., occurs only beyond the second critical voltage. Rubinstein's vortices appear in an array¹⁹ and have dimensions comparable to the diffusion layer. They, in fact, arrest the growth of the diffusion layer and stipulate its thickness. Dukhin's vortices, on the other hand, reflect the heterogeneity length scale and the radius of curvature of the surface and have only an indirect influence on the diffusion layer via its stirring. It is quite clear from the different voltage windows in Fig. 1, with different differential resistance in each region, that the nonlinear I - V characteristics of a nanochannel or nanoporous membrane is due to Rubinstein's vortex instability.

The considerable voltage drop across the polarized layer controls the I - V characteristics in the overlimiting region. Given a diffusion layer thickness, Ben and Chang¹⁶ and Yossifon *et al.*¹² offer a convenient estimate of the current density across the polarized layer in the absence of convec-

tion, for an ideal and a nonideal permselective membrane, respectively. The theory, however, still needs to be extended to the case with vortical convection in the overlimiting region to determine how the vortices select the diffusion layer thickness.

VI. WARBURG AND CHAOTIC IMPEDANCE

From the concentration-polarization layer structure of Fig. 5 a clear electroneutral diffusion region with a linear concentration profile is evident beyond the extended polarized layer. This diffusion layer is not necessarily established by tangential electro-osmotic (EO) or convection flow. Instead, it can extend to the electrode or be selected by the vortex instability. The relaxation time of this concentration front in the electroneutral diffusion layer is much longer than that in the polarized layer. As such, the dominant dynamics probed by impedance measurements at frequencies lower than 10 Hz correspond to the dynamics of this electroneutral diffusion front. For a symmetric electrolyte, one can eliminate the electromigration term by adding the cation and anion transport equations to produce a diffusion equation for the ion concentration C . Another equation, corresponding to net charge transport obtained by subtracting the anion transport equation from the cation equation, can be coupled to the diffusion equation to replace the two ion transport equations. However, for an electroneutral front, the second charge transport equation is irrelevant and the diffusion equation hence governs the dynamics leading to the linear concentration profile in the diffusion layer. For a constant counterion sink at the interface (mimics the cation permselective influx into the membrane), which was activated at time zero, the diffusion front from the diffusion equation is governed by²⁰

$$C(x,t) = C_\infty - \frac{S}{2\sqrt{D}} \left\{ 2 \sqrt{\frac{t}{\pi}} e^{-x^2/(4Dt)} - \frac{x}{\sqrt{D}} \left[1 - \operatorname{erf} \left(\frac{x}{2\sqrt{Dt}} \right) \right] \right\}. \quad (2)$$

In the limit of large $x^2/(Dt)$, this solution simplifies to $C(x,t) \sim C_\infty - (2St^{3/2}\sqrt{D}/x^2)e^{-x^2/4Dt}$. While the self-similar diffusive front has a concentration jump that is dependent on the flux S , the location of its front grows as \sqrt{Dt} independent of S . Provided the flux is varied slowly, this self-similar front evolution dynamics stipulates that the thickness of the diffusive front is well described by the simple and universal diffusive scaling \sqrt{Dt} , independent of the frequency and the instantaneous or rms electric field. We have monitored the front location of the fluorescent counterion dye with a low-frequency ac field and were able to verify this diffusive front dynamics,¹⁸ where the front breaks from the \sqrt{Dt} scaling (for frequencies <0.05 Hz, Fig. 7(b)) correspond to the onset of fully established vortices that are capable of arresting the diffusion layer growth.

This diffusive dynamics also occurs at high frequency and low voltages when there is very little polarization—when the period is much shorter than the charging time of the polarized layer at this low voltage. After Fourier transform, the concentration C assumes the form $C(x,\omega) \sim C_\infty + (C_0 - C_\infty)e^{-x\sqrt{\omega/D}}$, where C_0 is the concentration at the nanochannel-electrolyte interface. If there is very little electromigration, then the current at the surface ($x=0$) is entirely diffusive and the inverse impedance assumes the characteristic Warburg form with real and imaginary parts of the same amplitude at all frequencies,

$$\frac{1}{Z} = \frac{FA}{V} z \sqrt{D} (C_0 - C_\infty) \sqrt{i\omega} = \frac{FA}{V} z \sqrt{D} (C_0 - C_\infty) \sqrt{\omega/2} (1+i), \quad (3)$$

where A is the cross-section area of the nanoslot. This Warburg impedance is observed across many electrodes and its 45° phase is also observed in Fig. 3 at intermediate frequencies due to counterion diffusion fronts from the nanoslit.

The impedance spectrum is, however, very different at low frequencies and high voltage biases, as seen in Fig. 3. The lower applied voltages during the impedance measurement may not be able to sustain a stable vortex but it can produce fluctuating transient vortices. Similar chaotic current fluctuations at hydrodynamic time scales have also been observed in Ehlert and co-workers' experiments²¹ across a nanoporous granule.

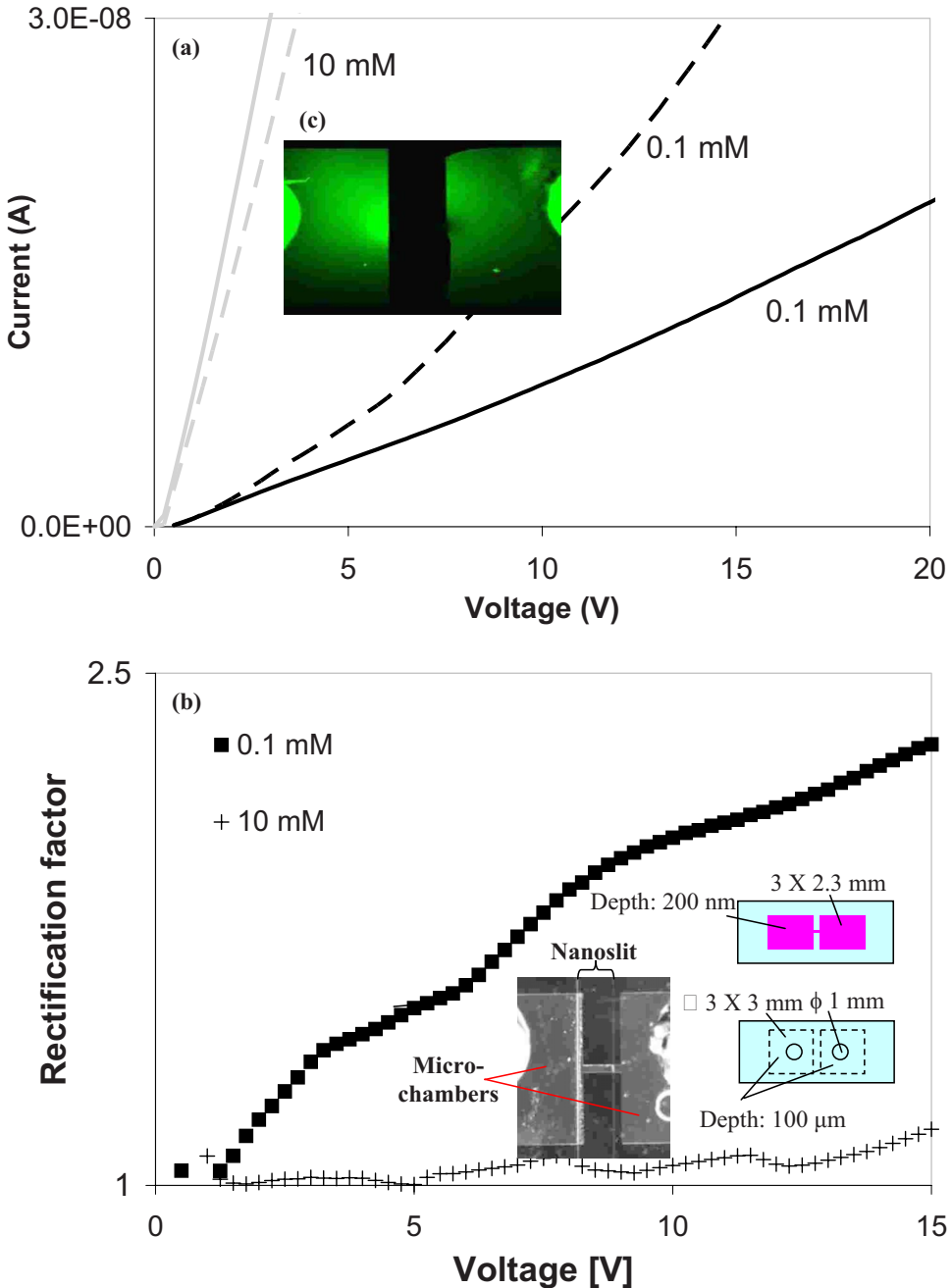


FIG. 8. Rectification of a nanoslit with asymmetric entrances. The left entrance is wider ($w=2.3$ mm) than the right ($w=0.1$ mm), as seen in the microscopic image (inset of (b)), and is obtained by intentional misalignment of the two Pyrex slides. The nanochannel height is $h=200$ nm and length is $d=0.5$ mm. (a) I - V measurements for varying ionic strengths and voltage bias (continuous line, anode at the right reservoir—reverse bias; dashed lines, anode at the left reservoir—forward bias); (b) the rectification factor defined as the ratio between the forward and reverse biases; (c) the depletion-enrichment phenomenon when the anode is at the right reservoir (enhanced online).

VII. RECTIFICATION

That the extended polarized layer only appears on the entry side of the membrane but not on the other side produces yet another anomalous I - V characteristic: current rectification, which is reminiscent of that occurring in a semiconductor bipolar diode. In Fig. 8, we depict the difference in the I - V curves when the polarity of the dc field is reversed for a nanoslit with asymmetric

entrances.²² As the flux-controlling polarized layer lies at opposite sides of the nanoslit with opposite polarity, the asymmetry of the entrance produces a significant current rectification result but only at high voltages beyond the critical voltage for the occurrence of the polarized layer. Earlier efforts to produce rectification at the low-voltage Ohmic region rely on inducing a nonhomogenous electrochemical potential along the nanochannel by introducing asymmetries in the nanochannel geometry (changing the channel height/pore diameter, i.e., the EDLs overlap) or surface functionalization.²³ Realizing that the asymmetric entrance of the polarized layer controls the current at high voltages has allowed us to produce rectification by simply changing the lateral dimension (i.e., channel spacing) at the two entrances, while keeping its height and surface charge homogeneous, or equivalently a homogeneous electrochemical potential. We note that the rectification effect disappears in the low-voltage Ohmic region when the polarized layer disappears.

This rectification phenomenon is very different from earlier ones for nanochannels with non-uniform channel height/pore diameter or surface functionalization. These earlier ones typically operate in the Ohmic region and rely on internal diodelike ratchet dynamics that most likely disappear at reasonably high throughputs. Here, the rectification results because the polarized layer only appears at the side where the counterions enter. Since the vortex instability that controls the overlimiting current occurs at a critical voltage that depends on the depth of the microreservoir, as the vortex instability involves length-scale-dependent viscous dissipation, different microreservoir depth at the two sides of a nanoslit with symmetric entrances would immediately introduce the rectification phenomenon at high voltages and throughputs.

As the polarized layer require some RC time to charge and discharge, it is not surprising that the hysteretic *I-V* cycle of Fig. 2 is scan-rate-dependent. The particular hysteresis pattern and its relationship to the polarized layer formation and dissipation dynamics remains to be explored. The capacitance estimated from the low-frequency limit of the impedance spectrum in Fig. 3 corresponds to the charging of the polarized layer at the entry surface. Since the polarized layer thickness is a function of voltage and changes discontinuously when the vortex instability sets in, this impedance signature should also be voltage-dependent. This nonlinear impedance characteristic also begs further examination.

VIII. SUMMARY AND FUTURE DIRECTIONS

All the curious ion flux characteristics here are observed without reaction. An internal reaction that consumes the counterions is expected to reduce the current once the threshold voltage for the reaction is exceeded. This may be a fruitful research direction, as a diodelike negative differential resistance can produce nonlinear inductor type characteristics. With a diode, the nanochannel resistance and the space-charge accumulating polarized layer capacitor can mimic many of the ion-channel electrophysiological dynamics, including unforced autonomous oscillations. If the dominant current-carrying counterions are being consumed by reaction at an electrode within the nanoslit, such oscillation can give rise to very sensitive molecular sensors whose detection signal is an unmistakable autonomous oscillation. Thoughts in the same direction may also lead to a viable interactive interface among biological systems, nanofluidics, and nanocircuitry. Both sensing and actuation are required for such an integrated system, and sensing of RNAs, growth factors, enzymes, and other molecular messengers for the cell is particularly pertinent.

One has to be mindful of extrapolating multiplicatively the *I-V* characteristics of a single channel to one with multiple channels or to a nanoporous membrane. In Fig. 9, we show that an array of nanoslits produces a current that is not an integer multiple of a single channel. The difference is believed to be caused by lateral communication among different polarized layers at the entry end. While communication is expected between two nanopores in a membrane, this is not necessarily so for an array of nanochannels (e.g., by simply increasing the channel spacing). This lack of channel communication could be exploited such that each channel can produce a unique impedance signal that can be picked up by a large electrode—there would not be cross-talk between the channels, thus allowing multitarget sensing by, for example, patterning each nanochannel with a different molecular probe.

Another clear distinction between nanochannels and nanoporous membranes is the tortuosity

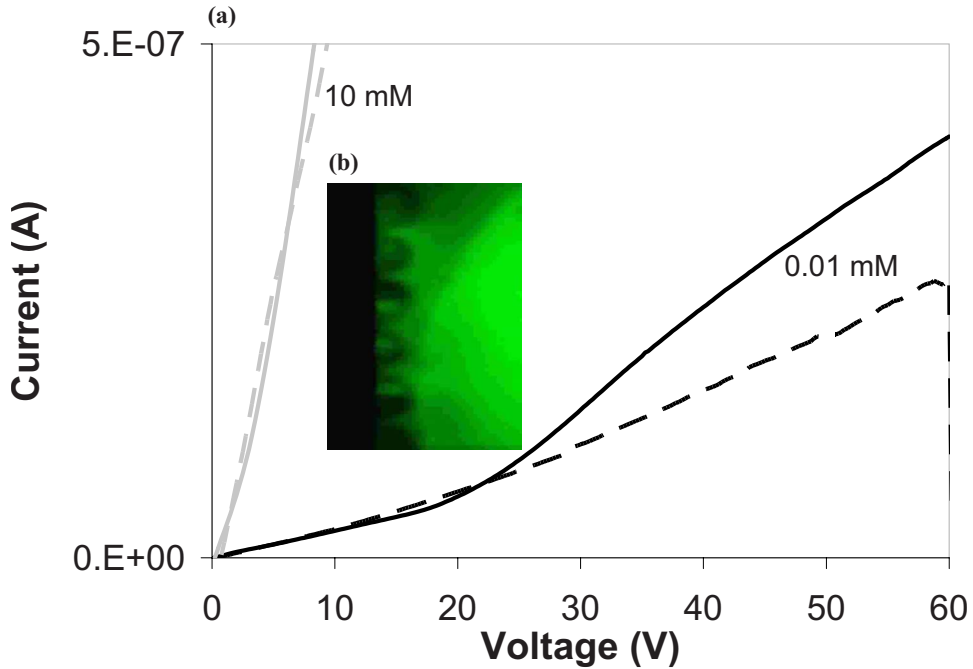


FIG. 9. Communication between neighboring nanochannels due to overlapping polarized layers at the entrance. (a) The current for a seven-channel array (solid) is compared to seven times that for a single-channel array (dashed) to determine the degree of communication (Reprinted with permission—Ref. 22). The single nanochannel dimensions are width $w = 0.1$ mm, height $h = 200$ nm, and length $d = 0.5$ mm. (b) An array of separate depletion regions emerging from the nanochannel array, just before their merging (enhanced online).

of void space in the latter. The counterion concentration is not uniform in a nanoporous membrane and there can be electroneutral pockets when the void dimension exceeds the Debye layer thickness. As a result, an osmotic pressure gradient exists along the field direction in a nanoporous membrane. Such a gradient is absent in a nanochannel. The same mechanisms that drive Rubinstein's instability and Dukhin's vortices can then produce internal closed vortices that reduce the void fraction for a net electro-osmotic flow. As such, hydrodynamic resistance in a nanoporous membrane probably exceeds that in a nanochannel by a large magnitude—one can get a robust ion current without any liquid flow. Even for a nanochannel, there is a large osmotic pressure gradient at the entrance that may introduce a critical voltage for electro-osmotic flow. To design a membrane that permits counterion flux but not electro-osmotic flow, which tends to convect cations as well, is a major design objective for permselective membranes. Selective filtration of charged molecules, like proteins and DNAs, by nanochannels will likely also benefit from the reduction in net liquid flow. Ion flux without imparting a body force on the liquid in a membrane is a classical example of irreversible thermodynamics and we may find ourselves revisiting this old field in the latest nanofluidic designs. Certainly, large ion pumps on the cell membrane do not permit significant water flux.

A related topic is multiphase flow in nanoporous membranes. Spinodal decomposition can occur in nanoslits due to surface charges, or air pockets can exist in an otherwise wet medium. In such cases, the conductivity is controlled by the connectivity of the more conducting phase. This conductivity, in turn, is determined by how the two phases coalesce and segregate under an electric field. The texture and connectivity of the two phase media are expected to be a strong function of the tortuosity and wettability of the medium. We suspect the hysteretic behavior observed in Fig. 2 is due to such two-phase flow and segregation/coalescence.

As mentioned in an earlier discussion on Faradaic currents, it would be interesting to combine such distinct voltage ringing and other nonlinear electrical properties of nanochannels with molecular sensing. Nanochannels can concentrate charged molecules and counterions. Molecular

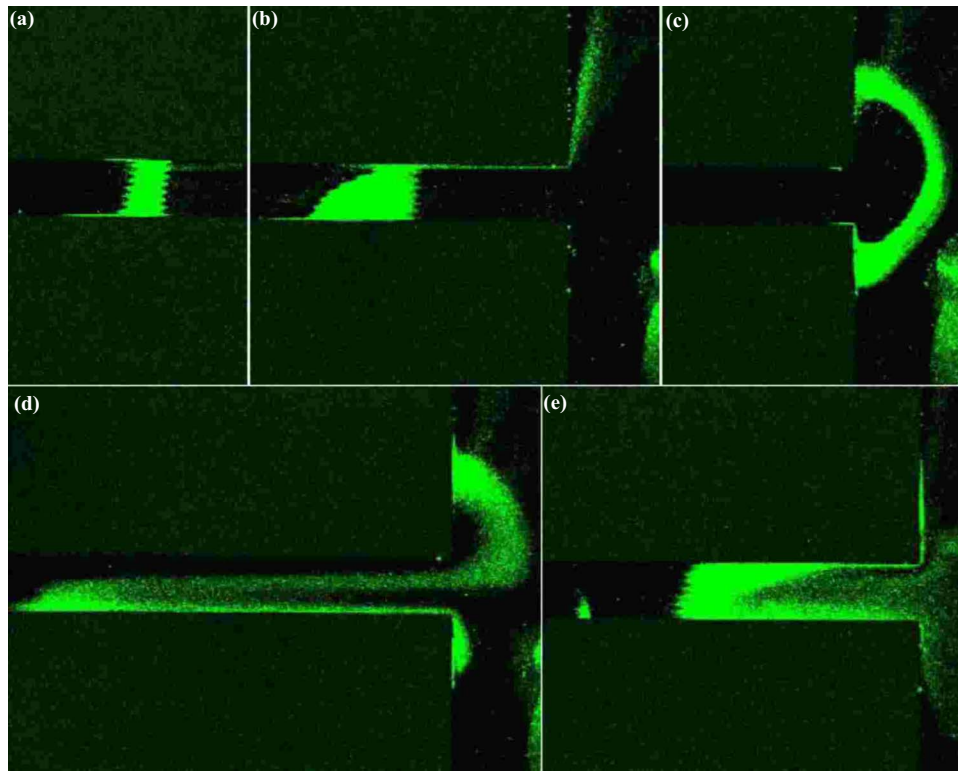


FIG. 10. Nanocolloids that assemble and disassemble within the nanochannel (width 100 μm and depth 200 nm) into a colloidal closed-packed structure (enhanced online).

gating has already been achieved by molecular probes at the nanochannel in some preliminary experiments, as in nanoporous beads for virus trapping.⁴ As shown in our recent analysis of nanocolloid dielectrophoresis,^{24,25} surface conduction becomes very important at nanoscales and surface conductance is known to be a sensitive function of molecular hybridization. If binding of such analytes with probes on the nanochannel surface can trigger potential oscillations due to the negative differential resistance (and positive feedback) of an imposed or intrinsic electrokinetic diode, it would allow very sensitive detection. In general, although biological electrophysiology typically operates in the nonlinear region with voltage gating and negative resistance, most impedance sensors still operate in the linear Ohmic region. Electrochemical sensors for molecular binding, in fact, show extensive rectification and cyclic voltammetric hysteresis across oxidation and reduction conditions. Other reversible Faradaic reactions with double-layer effects also show hysteretic behavior even without inverting the potential.²⁶ Coupling of such Faradaic nonlinear *I-V* responses to those of the nanochannel through some kind of ion Faradaic reaction at an internal electrode should produce extremely sensitive detection of molecular hybridization.

Even in the low-voltage Ohmic region, the intrachannel conductance can be a sensitive function of hybridization. Hybridization changes the active area of the nanochannel surface *A* for electron-transfer and surface conductance. This, in turn, produces a different Warburg impedance signal in Eq. (3) at high frequencies corresponding to the charge relaxation time at the entrance polarized layer, as the classical Warburg impedance theory omits space-charge effects.

Another fruitful integration would be with functionalized nanocolloids, which can be dispersed into a larger sample to capture target molecules^{27,28} and then sorted in large throughputs with a combination of nanochannel array, DEP, and microcross flow. Nanocolloids functionalized with molecular probes offer the advantage of being able to capture molecules in a high throughput flow with short diffusion time of the molecule to the colloid. However, as the fraction of hybridized nanocolloids is small for high-sensitivity detection, the challenge is then to sort the hybrid-

ized colloids from their unhybridized counterparts. This could be done by driving the hybridizing colloids in a flowing solution transversely into nanochannels with higher fields, as unlike unhybridized nanocolloids, hybridized nanocolloids could exhibit positive DEP at the proper frequency and hence favor the high-field nanochannels.²⁵ Charged nanocolloids behave like macroions but their significant volume and propensity to pack into colloid crystals in confined domains can produce nonlinear *I-V* and capacitance effects of their own when nanocolloids are trapped within nanochannels. The coupling between nanochannel *I-V* characteristics and the field-altering effects of packed nanocolloids may produce the most pronounced nonlinear *I-V* signals for nanocolloid capture. In Fig. 10, we show a preliminary experiment in this direction—nanocolloids are observed to assemble and disassemble periodically in a nanochannel.

In conclusion, we conjecture that the nonlinear *I-V* and impedance characteristics of nanochannels and nanoporous membranes reviewed in this expository will lead to a new sensing paradigm in diagnostic chips for molecular detection, with unprecedented sensitivity and specificity. However, to fully design such a new sensing platform, the underlying mechanisms must be fully understood.

ACKNOWLEDGMENTS

We would like to acknowledge the large number of collaborators and students who have advanced our understanding of ion transport in nanochannels and nanoporous membranes and our recent studies on nanocolloid DEP and molecular sensing: Y. Ben, S. Basuray, Y. Chang, Z. Chen, Z. Gagnon, P. Mushenheim, L. Floccare, F. Plouraboue, S. Senapati, P. Wang, S.-C. Wang, W. Wang, Y. Wang, and H.-H. Wei. Y. Chang and P. Mushenheim measured the impedance and *I-V* data. We are also grateful to Professor Y. Zhu and Professor A. Seabaugh for letting us use their facilities.

- ¹S.-C. Wang, H.-H. Wei, H.-P. Chen, M.-H. Tsai, C.-C. Yu, and H.-C. Chang, *Biomicrofluidics* **2**, 014101 (2008).
- ²P. Wang, Z. Chen, and H.-C. Chang, *Electrophoresis* **27**, 3964 (2006).
- ³Z. Chen, B. Boggess, and H.-C. Chang, *J. Mass Spectrom.* **42**, 244 (2007).
- ⁴Z. Chen, F.-C. Hsu, D. Battigelli, and H.-C. Chang, *Anal. Chim. Acta* **569**, 76 (2006).
- ⁵T. M. H. Lee, M. Carles, and I.-M. Hsing, *Lab Chip* **3**, 100 (2003).
- ⁶J. Yang, F. Lu, L. W. Kostiuk, and D. Y. Kwok, *J. Nanosci. Nanotechnol.* **5**, 648 (2005).
- ⁷D. Stein, M. Kruthof, and C. Dekker, *Phys. Rev. Lett.* **93**, 035901 (2004).
- ⁸M. Ali, V. Bayer, B. Schiedt, R. Neumann, and W. Ensinger, *Nanotechnology* **19**, 485711 (2008).
- ⁹S. J. Kim, Y. C. Wang, J. H. Lee, H. Jang, and H. Han, *Phys. Rev. Lett.* **99**, 044501 (2007).
- ¹⁰N. Lakshminarayanaiah, *Membrane Electrodes* (Academic, New York, 1976).
- ¹¹J. Keener and J. Sneyd, *Mathematical Physiology* (Springer, New York, 2009).
- ¹²G. Yossifon, P. Mushenheim, Y.-C. Chang, and H.-C. Chang, “Nonlinear *I-V* characteristics of nano-pores,” *Phys. Rev. E* (submitted).
- ¹³V. G. Levich, *Physicochemical Hydrodynamics* (Prentice-Hall, New York, 1962).
- ¹⁴S. S. Dukhin, *Adv. Colloid Interface Sci.* **35**, 173 (1991).
- ¹⁵I. Rubinstein and L. Shtilman, *J. Chem. Soc., Faraday Trans. 2* **75**, 231 (1979).
- ¹⁶Y. Ben and H.-C. Chang, *J. Fluid Mech.* **461**, 229 (2002).
- ¹⁷I. Rubinstein, E. Staude, and O. Kedem, *Desalination* **69**, 101 (1988).
- ¹⁸G. Yossifon and H.-C. Chang, *Phys. Rev. Lett.* **100**, 254501 (2008).
- ¹⁹I. Rubinstein and B. Zaltzman, *Phys. Rev. E* **62**, 2 (2000).
- ²⁰R. J. Hunter, *Foundations of Colloid Science* (Clarendon, Oxford, 1989), Vol. 2.
- ²¹S. Ehlert, D. Hluskou, and U. Tallerek, *Microfluid. Nanofluid.* **4**, 471 (2008).
- ²²G. Yossifon, Y.-C. Chang, and H.-C. Chang, “Rectification, gating voltage and interchannel communication of nanoslot arrays due to asymmetric entrance space charge polarization,” *Phys. Rev. Lett.* (submitted).
- ²³I. Vlassiouk and Z. S. Siwy, *Nano Lett.* **7**, 552 (2007).
- ²⁴S. Basuray and H.-C. Chang, *Phys. Rev. E* **75**, 060501 (2007).
- ²⁵H.-C. Chang, *AIChE J.* **53**, 2486 (2007).
- ²⁶O. Orlychenko, Y. Ye, and H.-C. Chang, *Phys. Rev. E* **57**, 5196 (1998).
- ²⁷I.-F. Cheng, H.-C. Chang, D. Hou, and H.-C. Chang, *Biomicrofluidics* **1**, 021503 (2007).
- ²⁸J. Gordon, Z. Gagnon, and H.-C. Chang, *Biomicrofluidics* **1**, 044102 (2007).